The Tangential Nucleus Controls a Gravito-inertial Vestibulo-ocular Reflex

The tangential nucleus controls a gravito-inertial vestibulo-ocular reflex.

Short title: A fundamental gaze-stabilization circuit.

Authors: Isaac H. Bianco[*1], Leung-Hang Ma[*2], David Schoppik[*1], Drew N. Robson[1], Michael B. Orger[3], James C. Beck[2], Jennifer M. Li[1], Alexander F. Schier[1], Florian Engert[1§], Robert Baker[2].

[*] *authors contributed equally*
§ *author for correspondence*

Affiliations: [1] Department of Molecular and Cellular Biology and Center for Brain Science, Harvard University, Cambridge, MA, USA; [2] Department of Physiology and Neuroscience, New York University School of Medicine, NY, USA; [3] Champalimaud Centre for the Unknown, Lisbon, Portugal.

v 2.8 | Current Biology | neuron.bst

Summary

Whilst adult vertebrates sense changes in head position using two classes of accelerometer, at larval stages zebrafish lack functional semicircular canals and rely exclusively on their otolithic organs to transduce vestibular information. Despite this limitation, they perform an effective vestibulo-ocular reflex (VOR) that serves to stabilize gaze in response to pitch and roll tilts. Using single-cell electroporations and targeted laser-ablations, we identified a specific class of central vestibular neurons, located in the tangential nucleus, which are essential for the utricle-dependent VOR. Tangential nucleus neurons project contralaterally to extraocular motoneurons, and in addition, to multiple sites within the reticulospinal complex. We propose that tangential neurons function as a broadband inertial accelerometer, processing utricular acceleration signals to control the activity of extraocular and postural neurons, thus completing a fundamental three-neuron circuit responsible for gaze stabilization.

Introduction

To stabilize gaze in response to movements of the head/body, vertebrates process vestibular signals to produce compensatory eye rotations of equal and opposite velocity (the vestibulo-ocular reflex, or VOR). In primates, the VOR is almost perfectly compensatory and studies of the underlying neural circuitry have uncovered general principles regarding the organization of circuits mediating sensorimotor transformations (Goldberg & Fernández, 2011). The larval zebrafish is a genetic model organism that produces eye rotations in response to changes in head orientation from as early as 4 days of age (Moorman et al., 1999; Mo et al., 2010). Due to their small size, the semicircular canals are not functional until fish are approximately one month old (Beck et al., 2004b; Lambert et al., 2008). Analysis of *monolith* mutant larvae, which can be reared with only a single functional otolithic organ, has demonstrated that whilst the saccule appears dispensable for vestibular sensitivity, the utricle is essential for vestibular behaviors and indeed for survival of the larval animal (Riley & Moorman, 2000). Studies of the rotational VOR in mammals suggest that otolithic organs function poorly at even modestly high frequencies and primarily serve to enhance the semicircular canal-ocular reflex for low frequency earth-horizontal rotations (Angelaki & Hess, 1996). Earlier studies of vestibular eye movements in zebrafish were ambiguous with respect to the axis of vestibular stimulation (Mo et al., 2010) or did not exclusively drive the vestibular system (Moorman et al., 1999) and therefore the extent to which larval zebrafish can produce a compensatory VOR with only utricular input, remains unknown.

The VOR is primarily mediated by a "three-neuron arc", a classic anatomical circuit that comprises 1) a primary afferent neuron, which conveys signals from hair cells in the inner ear associated with changes in head position, 2) a second-order vestibular neuron, which processes

the afferent input and projects to 3) an ocular motoneuron, which innervates extraocular muscles to drive gaze-stabilizing counter-rotations of the eye (Szentagothai, 1950). Previous work in teleost fish has described both primary afferent neurons (Haddon & Lewis, 1996) and the ocular motoneurons (Graf & McGurk, 1985). However, the specific second-order vestibular neurons that mediate the sensorimotor transformations underlying specific vestibular reflexes remain unidentified. Neurons in the tangential nucleus, first described by Cajal, possess anatomical (Cajal, 1908) and physiological (Suwa et al., 1999) properties conducive to central vestibular function, but have not been shown to play a functional role in any behavior. In addition to vestibular input, circuits involved in the mammalian VOR are thought to integrate visual information, both as a means of resolving sensory ambiguities (Angelaki & Cullen, 2008), and driving plasticity (Miles & Lisberger, 1981). Similarly to mammals, larval zebrafish rely heavily on their visual system, but multimodal integration to drive behavior has not been described.

The larval zebrafish thus affords a unique opportunity to identify a complete circuit, driven by input from the first operational vestibular sensor, and to discover the computations which transform stimulus to behavior. We first characterized the performance and ontogeny of the VOR in larval zebrafish in response to both static and dynamic rotational stimuli, demonstrating compensatory eye rotations of surprising high performance and that operate over a broad frequency range. Surgical ablations showed that signals from the left and right utricles are combined linearly by the central circuitry controlling the VOR such that both end-organs contribute equally to the response of each eye. Furthermore, changes in primary eye position predicted a distinct pattern of connectivity for central vestibular neurons. We identified such neurons within the tangential nucleus and, using laser-ablation, demonstrated the necessity of this specific class of vestibular neuron for the utricle-dependent VOR. Finally, we discovered that visual input interacts with vestibular signals to enhance ocular compensation, suggesting that sensory feedback signals which guide motor learning are present and functional in the larval zebrafish. Taken together, our findings define the larval zebrafish VOR, from rotational stimuli to neural computations to compensatory, conserved behavior.

Results

Larval zebrafish produce compensatory eye movements in response to head rotations

To stabilize gaze (i.e. minimize retinal slip) in the face of changes in head/body orientation, the vestibular system must drive compensatory eye rotations of equal and opposite velocity. How well can larval zebrafish, which have only one functional vestibular sense organ, stabilize their gaze?

To resolve this issue, we designed an apparatus (Fig. S1) in which partially restrained larvae were pitch-tilted (i.e. nose up/down) about an earth-horizontal interaural axis centered on the ear

(Fig. 1a). The appropriate compensatory responses are torsional eye rotations (ψ in Fig. 1b), which we measured under infra-red illumination in the dark using a high-speed camera and automated feature detection software. We first presented larvae with step changes in head position, allowing us to evaluate both static changes in primary eye position, which represent an otolith-ocular response to changes in head orientation relative to gravity termed 'counter-rolling', as well as dynamic responses of the eye to head rotations at a range of head positions. We presented cycles of 10° steps from $-60°$ (nose-up) to $+60°$ (nose-down) (Fig. 1c); individual steps comprised a rapid change in angular position (duration 0.5 s, peak velocity 32°/s) followed by a stationary period at the new position (duration 4.5 s). These values were chosen based upon a preliminary evaluation of the oculomotor range and are comparable to prior studies in goldfish (Pastor et al., 1992).

Larval zebrafish exhibited an ocular counter-rolling response which we quantified by determining primary torsional eye position (averaged over the final 3 s of each step) as a function of head position. There was an approximately linear relationship between eye position and head rotation over the range $\pm 40°$ (Fig. 1d). However, at more eccentric pitch tilts, torsional eye position approached a plateau, as the mechanical limits of globe rotation and/or the biophysical sensitivity of the utricle were reached.

In response to the rapid change in angular head position at the beginning of each step, the eye showed a torsional counter-rotation followed, in some cases, by a decay to a new primary eye position. Comparing velocity profiles of the eye and the step stimulus revealed that this dynamic rotational VOR response showed a strong dependence on head position (Fig. 1e). The three steps that tilted the fish nose-upwards, away from the horizontal (0 to $-30°$), resulted in eye rotations with a high peak velocity, comparible to that of the step. At more eccentric positions, peak eye velocity was considerably reduced, and eye position followed a simple sigmoidal profile.

To quantify the extent to which eye rotations were compensatory, we calculated the gain of the response as the ratio of peak eye velocity to peak head velocity (32°/s). A gain of 1 implies eye movements can fully compensate for head rotation and therefore fully eliminate retinal slip. In the example shown in Figure 1, during rotation away from the horizontal, gain approached and even exceeded 1, indicative of a highly effective compensatory VOR (Fig. 1f).

In summary, in the absence of functional semicircular canals, larval zebrafish perform a utricle-specific rotational VOR that in some cases can fully compensate for changes in head/body pitch.

Ontogeny and bandwidth of the larval zebrafish VOR

Between 3 and 4 dpf, larval zebrafish undergo a profound change in posture and locomotor behavior as they transition from lying immobile on their side to swimming upright (Kimmel

et al., 1995). To quantify VOR development over the same time frame (Riley & Moorman, 2000; Mo et al., 2010), we measured eye rotations in response to pitch-tilts in larvae from 3 to 10 days post-fertilization (dpf). We expanded our stimulus set to include sinusoidal oscillations with constant peak velocity (15.7°/s) between 0.0625 Hz and 2 Hz, enabling us to characterize the frequency range (i.e. bandwidth) of the utricular VOR. This peak angular velocity was selected based upon a preliminary characterisation of VOR performance (Fig. S2) and was compatible with the range of sinusoidal stimuli our apparatus could deliver. At each frequency, the performance of eye movements was measured by calculating the gain (ratio of amplitude of eye rotation to head rotation) and the phase difference between the vestibular stimulus and the ocular response.

Three-day-old larvae failed to show any torsional eye rotations at any of the sinusoidal frequencies we tested. However, from 4 dpf, larvae showed a rotational VOR with similar performance across the entire frequency range (Fig. 2a–c). The mean gain across frequencies increased significantly from 4 dpf (0.24 ± 0.01, mean $\pm$ s.e.m.) to 5 dpf (0.33 ± 0.01, $p < 0.05$), and did not improve further at 10 dpf (0.31 ± 0.01, $p > 0.05$). The phase profiles of the ocular responses were similar between 4 and 10 dpf (Fig. 2c): At all ages, a phase lag was observed at frequencies above 0.5 Hz, which became as high as 40° at 2 Hz.

To complete our characterization of the ontogeny of the VOR, we presented brisk step changes in pitch-tilt to larvae of different ages (Fig. 2d, e). At 3 dpf, there was no oculomotor response following step changes in head pitch, in agreement with the absence of response to sinusoidal rotations. However, from 4 dpf, larvae responded to step changes in pitch and the magnitude of the response increased with age. At 10 dpf, the mean gain of the VOR in response to nose-up tilts away from the horizontal approached 1, with a slight anisotropy and reduced gain for nose-down rotations (Fig. 2e).

In summary, the zebrafish VOR develops at an ethologically relevant age, between 3 and 4 dpf, when larval fish first start to locomote in their environment. From the outset, the utricle confers responsiveness to a surprisingly broad range of frequencies, allowing compensatory eye movements in the absence of input from the semicircular canals.

Linear summation of independent utricular signals

The naturally isolated otolithic system in zebrafish offers a unique opportunity to study how bilateral utricular information is combined by the central circuitry controlling the VOR. We independently inactivated the left and right utricles of 5 dpf larvae by surgically removing the utricular otoliths (Fig. 3a, b) and subsequently determined VOR performance by measuring responses to sinusoidal pitch-tilts (Fig. 3c, d).

After unilateral otolith removal, gain dropped across all frequencies to approximately half of its level pre-surgery. For the left eye, mean gain decreased to $51.3 \pm 2.8\%$ of its level pre-surgery,

which does not differ significantly from 50% (t-test, $p = 0.64$). For both the left and right eye, the deficit was similar following removal of either the left or right otolith ($p > 0.05$ for left versus right otolith, for both eyes), indicating that both utricles contribute equal drive to each eye. As expected in an exclusively utricle-driven system, bilateral removal of both utricular otoliths completely abolished pitch-tilt evoked movements of both eyes (mean left eye gain $= 0.01 \pm 0.006$, right eye gain $= 0.01 \pm 0.006$, $p > 0.05$ for left versus right eye). Sham surgeries, which collapsed the otic vesicle but left the otoliths untouched, resulted in minimal effects across all frequencies, demonstrating that changes in VOR performance were due to removal of the utricular otoliths but not general damage to the otic vesicle (Fig. S2 and Movie S1). We conclude that inputs from the left and right utricles are equal in strength and are combined in an additive manner, with each able to drive both eyes at half of normal gain.

Intriguingly, after bilateral otolith removal, all larvae performed torsional eye rotations with low gain when pitch-tilt stimuli were presented in the light (Fig 3c, d), demonstrating that the eye's ability to rotate was still intact. We interpret these eye movements as a torsional optokinetic response (Huang & Neuhauss, 2008) and note that for these visually evoked eye rotations, the phase of the ocular response shifts considerably as the frequency of head rotation increases, a hallmark of the slower response of the visual system.

Changes in primary eye position following unilateral otolith removal predict contralateral connectivity of central vestibular neurons

The reduction in gain following unilateral utricle inactivation is compatible with a loss of drive to either the superior and/or inferior ocular muscles that mediate torsional eye rotations. To obtain insights into the organisation of the utricle-specific VOR circuit, we measured changes in primary vertical eye position, where tone of the superior and inferior eye muscles can be more clearly inferred.

We quantified vertical eye position by imaging the fish head-on (Fig. 4 and Movie S2). In intact larvae, there was a slight upward bias in the visual axis of both eyes, suggesting tone in the superior eye muscles is normally elevated. Following removal of the left utricular otolith, the vertical axis of both eyes rotated clockwise (i.e. the upper pole of both eyes rotated towards the side of the lesion), indicative of reduced activity of superior eye muscles on the left and inferior eye muscles on the right. A symmetrical result was observed if we removed only the right otolith. Bilateral removal of the otoliths resulted in both eyes adopting a near-vertical orientation, compatible with a loss of tone in superior as well as inferior muscles on both sides.

These changes in ocular muscle tone suggest a circuit organisation in which utricular signals control the activity of superior eye muscles on the same side of the head and inferior eye muscles on the opposite side. Given that superior and inferior eye muscles are controlled by contralateral

and ipsilateral extraocular motoneurons, respectively (Graf & McGurk, 1985), our behavioral data predicts the existence of central vestibular neurons that receive utricular input and project across the midline to relay the vestibular signal to ocular motoneurons on the opposite side of the brain.

Neurons within the tangential nucleus project to contralateral ocular motoneurons

Next, we sought to identify second-order neurons within the utricle-specific VOR circuit. In teleost fish, amphibians, reptiles and birds, the tangential nucleus represents a discrete neuronal cluster within hindbrain rhombomere 5 (Cajal, 1908). Because this nucleus receives a dense utricular input (Straka & Baker, 2011) and tangential neurons, unlike other classes of vestibular neuron, modulate their firing in response to static head displacements, indicative of physiological sensitivity to signals from otolithic end-organs (Suwa et al., 1999), we hypothesised that the tangential nucleus might be the site of second-order neurons controlling the VOR.

We used focal electroporation to label individual tangential neurons in rhombomere 5, adjacent to the otic vesicle, with a construct driving expression of membrane-tethered GFP. In addition, we retrogradely labeled the reticulospinal complex and the ocular motoneurons using fluorescent dextrans. We verified that retrograde tracing from the orbit effectively labeled the oculomotor and trochlear nuclei by performing a control tracing experiment in the Tg(*isl1*:GFP)^{rw0} transgenic larva, in which the majority of the cranial motor nuclei are labelled (Higashijima et al., 2000) (Fig. S3). The combination of focal electroporation and retrograde dye tracing allowed us to image the entire morphology of individual tangential neurons and define their axonal projection patterns (Fig. 5). We identified three morphologically distinct subtypes of tangential neuron in the 5–6 dpf larval zebrafish brain, which we term "Ascending", "Ascending/Descending" and "Commissural". Their projection patterns are summarized in Figure 5g.

Compatible with these neurons receiving direct utricular inputs (Straka et al., 2001, 2003), all of the tangential neurons that we labeled ($n = 16$) extended a dendritic arbor in the octavolateral neuropil at the lateral border of the hindbrain, where afferent axons from the otic vesicle terminate (Highstein et al., 1992; Tomchik & Lu, 2005). All three subtypes projected their axons to the contralateral side of the brain, consistent with the functional prediction from the effects of otolith removal on ocular muscle tone, described above. The Ascending subtype (Fig. 5a, c, e; Movie S3; $n = 7/16$) projected an axon across the midline which then turned rostrally within the medial longitudinal fasciculus (MLF) and formed terminal arbors within the trochlear nucleus (nIV), the oculomotor nucleus (nIII) and the nucleus of the medial longitudinal fasciculus (nMLF). The Ascending/Descending subtype (Fig. 5b, d, f; Movie S4; $n = 6/16$) had an axon that bifurcates after crossing the midline. One collateral extends rostrally to innervate nIII, nIV and the nMLF, similar to the Ascending subtype (Fig. 5f), while the second collateral extends caudally to reach the rostral spinal cord. Notably, for this subtype we observed multiple axonal arborizations in the

vicinity of reticular neurons in hindbrain rhombomeres 4–8. The Commissural subtype (Fig. 5b, d; $n = 3/16$) projected an axon directly across the medio-lateral axis of the hindbrain to the region of the contralateral tangential nucleus and elaborated extensive arbors within both the ipsilateral and contralateral octavolateral neuropil. In contrast to other tangential neurons, this subtype did not project towards ocular motoneurons.

In summary, two of the three subtypes of tangential neuron we identified in larval zebrafish — Ascending and Ascending/Descending — have a morphology predicted by unilateral utricle inactivation experiments. These neurons receive dendritic inputs in the region of the hindbrain where utricular afferents terminate and project contralaterally to oculomotor nuclei and are therefore good candidates to complete a three-neuron arc mediating the VOR.

Tangential neurons are required for the utricular VOR

To test whether tangential neurons were necessary for the VOR, we measured oculomotor performance before and after laser-ablation of neurons in the tangential nuclei. To enable selective targeting of these neurons, we generated transgenic larvae that pan-neuronally expressed two proteins: a membrane-tethered red fluorescent protein (lyn-mCherry) to reveal the architecture of the hindbrain reticular scaffold (Fig. 6a), as well as a photo-activatable form of GFP (C3PA-GFP; Ruta et al., 2010). Using a two-photon microscope, we selectively photo-activated C3PA-GFP in a small volume of ventro-lateral rhombomere 5, which resulted in bright labeling of 20–25 cells on each side of the hindbrain (Fig. 6b). Photo-labeled axons ascended in the MLF and projected arbors within the oculomotor and trochlear nuclei as well as the in nMLF, just as we had observed for individually electroporated tangential neurons (Fig. 6c, compare to Fig. 5g).

Our photo-labeling method allowed individual targeting of tangential neurons for ablation using a pulsed infrared laser. Selective ablation of single zebrafish neurons has been reported previously using this technique, and causes little or no damage to immediately adjacent cells (Orger et al., 2008, and Fig. S5). We targeted all of the labeled neurons on both sides of the hindbrain (Fig. 6d) and compared VOR responses to sinusoidal pitch-tilts before and after ablation. Larvae showed an almost 60% decrease in the gain of the VOR following laser ablation (Fig. 6e) and this effect was similar across all the frequencies tested (mean gain across frequencies under baseline conditions $= 0.39 \pm 0.010$, after ablation $= 0.16 \pm 0.011$, $p < 0.001$, $n = 12$). In two larvae that showed the most complete loss of VOR performance, we provided visible illumination to the fish and observed torsional eye rotations (Fig. 6f, red lines) of similar amplitude to those observed following bilateral utricle removal (Fig. 3d, red lines). These visually-evoked ocular counter-rotations, as well as our observation of spontaneous saccades (data not shown) demonstrate that laser-ablations targeted to tangential neurons do not directly affect the ability of the fish to rotate their eyes, but specifically impair the VOR.

These loss-of-function experiments demonstrate that the tangential nucleus contains central vestibular neurons that are essential for the larval zebrafish rotational VOR.

Dynamic interactions between visual and vestibular signals in the control of compensatory eye movements

Following utricular inactivation and tangential nucleus ablation, we observed a visually-evoked torsional optokinetic response when fish were pitch-tilted in the light. To investigate how the oculomotor system combines visual input with utricle-derived vestibular signals, we designed a stimulus paradigm that set these inputs in opposition to one another: When larvae are mounted upside-down and then pitch-tilted in the light, the direction of hair cell deflection in the utricle is reversed, whereas the direction of retinal slip is unchanged (Fig. 7a).

When larvae were inverted and stimulated with sinusoidal pitch-tilts in the dark, they showed torsional eye rotations in the opposite direction to when they were mounted upright (Fig. 7b and Movie S5). Whilst gain was similar between upright and inverted conditions, phase differed by 180°, reflecting the 180° shift in utricular drive (Fig. 7c). When inverted larvae were pitch-tilted in the light, eye movements continued to show reversed directionality but gain was strongly modulated by sinusoidal frequency. At lower sinusoidal frequencies, gain was greatly reduced, compatible with the integration of two sensory signals of opposite sign (Fig. 7b, c; $p < 0.05$ in 4 out of 4 larvae, 0.0625–0.25 Hz). However, at higher frequencies, gain exceeded that measured under normal, upright, conditions ($p < 0.05$ in 3 out of 4 larvae at 2 Hz). This phenomenon at higher frequencies can be explained by the summation of two signals, visual- and utricular in origin, which have opposite signs and differ in phase by $> 60°$; this will result in an additive signal of greater amplitude than either of the two original sinusoids alone. A phase difference exceeding 60° is likely because following bilateral otolith removal we observed that the optokinetic response showed a large phase shift approaching 100° at 2 Hz (Fig. 3d).

These data demonstrate that visual inputs have the capacity to modulate utricle-driven torsional eye movements and that the central circuitry underlying the VOR combines signals across multiple modalities.

Discussion

The fact that vestibular sensitivity of the larval zebrafish is conferred exclusively by the utricle has enabled us to delineate the first functional neural circuit controlling gaze stabilization. Despite lacking head velocity signals from the semicircular canals, larval zebrafish produce compensatory ocular counter-rotations that, under some conditions, are likely to eliminate retinal slip and perfectly stabilize gaze. We propose that central vestibular neurons in the tangential nucleus

represent the essential second-order neurons that process utricular acceleration signals and control the activity of ocular motoneurons on the opposite side of the brain, which in turn drive the eye muscles. This simple three-neuron pathway can be considered a fundamental circuit responsible for gaze stabilization (Fig. 8). This circuit parallels the recently elucidated set of neurons responsible for horizontal saccades (Schoonheim et al., 2010); these neurons control the medial and lateral rectus muscles, which do not participate in the torsional eye rotations underlying the larval zebrafish VOR. We show that torsional eye movements can be modulated by visual signals, indicating that pathways processing other modalities converge with the core otolith-ocular circuit. Furthermore, later in development, input from the semicircular canals must be incorporated within an existing otolithic template.

Over the same developmental time-course during which larval zebrafish begin to swim upright, they develop utricle-dependant otolith-ocular reflexes in response to changes in head/body orientation. Larvae showed a static counter-rolling response that changed primary torsional eye position as a function of head orientation, similar to that described by Moorman et al. (1999). In addition, we demonstrated that the utricle mediates a rotational VOR with sensitivity to head orientation in a manner that is comparable to adult animals presented with similar stimuli (Hess & Dieringer, 1990; Maruta et al., 2001; McArthur & Dickman, 2008). Studies in which surgical interference was used to dissociate the contribution of each vestibular end-organ have suggested that the semicircular canals are predominant and drive the VOR across a wide range of frequencies, while the utricle secondarily augments the VOR at low frequencies (below ~ 0.1 Hz; Angelaki & Hess, 1996). However, we find that the VOR circuitry in larval fish uses utricular input alone to drive compensatory eye movements across a surprisingly broad range of frequencies, from $1/16^{\text{th}}$ Hz to 2 Hz. A possible explanation is that in larval zebrafish we could quantify the behavioral output of a circuit that naturally receives sensory input from a single vestibular end organ whereas perturbation studies in adult vertebrates inevitably disrupt mature circuits that have adjusted during development to combine input from both otolithic organs and the semicircular canals. Although larvae were not able to fully eliminate retinal slip (i.e. gains of 1) in response to our sinusoidal stimuli (peak velocity $15.7^\circ/s$), gains could meet or exceed 1 during step stimuli (peak velocity $32^\circ/s$), suggesting head movements are better compensated at a higher angular velocity range. Because larval fish swim in rapid bouts, with turns characterized by high peak angular velocities (Budick & O'Malley, 2000; Burgess & Granato, 2007), it seems appropriate that the larval VOR circuit should be tuned to higher velocities.

By combining molecular-genetic and optical techniques in larval zebrafish, we identified a specific subset of central vestibular neurons, located in the tangential nucleus, as being essential for the utricle-dependent VOR. Electrophysiological recordings in amphibians, as well as electron microscopy ultrastructural studies in chicks, have demonstrated that tangential nucleus neurons

are second-order vestibular neurons, receiving a direct (monosynaptic) utricular input (Straka et al., 2003; Peusner & Morest, 1977). Otolithic afferents primarily encode net gravitational and inertial acceleration (Fernández & Goldberg, 1976), providing the tangential nucleus with an appropriate signal to act as a broadband gravito-inertial accelerometer mediating otolith-ocular reflexes. Our loss-of-function experiments, in which we precisely laser-ablated individually photo-labeled neurons, demonstrated, for the first time, the functional necessity of the tangential nucleus for processing acceleration signals to guide VOR behavior.

The morphologies of the tangential neurons we identified are largely similar to tangential nucleus neurons in adult teleosts, amphibians and birds (Suwa et al., 1999; Straka et al., 2001; Gottesman-Davis & Peusner, 2010) and to medial vestibular nucleus neurons in mammals (Büttner-Ennever & Büttner, 1992). Two subtypes projected from the octavolateral region of the hindbrain, where utricular afferent axons terminate, to contralateral ocular motonuclei (nIII and nIV) that drive the torsional eye rotation responses to pitch tilts (see Fig. 8). The changes in vertical eye position, following unilateral otolith removal, provide strong support for functional connectivity between the contralateral axonal arbors of tangential neurons and the extra-ocular motoneurons in nIII and nIV. The linear summation of left and right utricular inputs for the VOR is explained by this circuit organization: Torsional rotations are driven by the combined activity of one superior and one inferior ocular muscle (see Fig. S1) and each utricle provides (through the tangential nucleus) input to one member of the pair: the superior muscle in the case of the ipsilateral eye and the inferior muscle of the contralateral eye. Thus, we propose that a specific subtype of central vestibular neuron, located in tangential nucleus, represents the second-order neuron that completes a fundamental three-neuron arc that underlies a utricle-dependent VOR early in vertebrate development, before the semicircular canals attain functionality.

In addition to the two morphological subtypes of tangential neuron that projected to ocular motonuclei, we also observed a Commissural subtype that projected to the region of the contralateral tangential nucleus. Bilateral interconnections between vestibular nuclei enable push–pull interactions between reciprocal semicircular canal pairs that increase the sensitivity of second-order vestibular neurons and, in addition, are important for velocity storage (Highstein & Holstein, 2006). Physiological evidence exists for both excitatory and inhibitory commissural connections within the otolithic system of mammals and has been suggested to provide a mechanism for increasing the sensitivity of vestibular neurons to linear acceleration and head tilt (Angelaki, 2004; Uchino et al., 2001); our identification of Commissural tangential neurons suggests similar circuitry exists for processing of utricular signals in larval zebrafish.

Natural gaze stabilization is not solely achieved by ocular compensation, but by the combined responses of the eye, head and body to vestibular stimuli; these responses are often mediated by the coordinated activity of distinct neuronal populations (Pompeiano & Allum, 1988). Intriguingly,

in addition to innervating oculomotor nuclei, tangential nucleus neurons project strongly to the nucleus of the medial longitudinal fasciculus (nMLF) and extend axonal arbors in the vicinity of reticulospinal neurons in r4–8. In larval zebrafish, activity of the nMLF and other reticulospinal neurons is correlated with swimming (Orger et al., 2008), while occipital and pectoral motoneurons in r8 control axial and fin musculature, respectively (Ma et al., 2010). Thus, the projection patterns of individual tangential neurons support the idea that the tangential nucleus processes sensory input from the utricle and coordinately controls both ocular responses and posture in order to stabilize gaze. This "double-duty" is consistent with the small number of neurons present in the larval zebrafish brain, and is a likely candidate for further refinement as the animal ages.

The vestibular system of larval fish, which is entirely dependent on sensory input from a single end-organ, faces a profound limitation. Otolithic organs, as sensors of both gravitational and inertial acceleration, are unable to distinguish between changes in head orientation with respect to the earth's gravitational force vector (e.g. the head tilting backwards) versus translational acceleration (e.g. walking forwards) (Angelaki & Cullen, 2008). Current models and physiological data suggest that the semicircular canals, as sensors of angular acceleration, play a crucial role in resolving this "tilt-translation illusion" (Angelaki et al., 1999; Hess & Angelaki, 1999; Angelaki et al., 2004). In the absence of canal inputs, how might zebrafish larvae disambiguate utricular signals? Our data demonstrate that visual input is sufficient to drive torsional eye rotations in the absence of a functional VOR circuit (either after bilateral utricle inactivation or tangential nucleus ablation), demonstrating that, as has been shown for other species, zebrafish larvae show a torsional optokinetic response (Huang & Neuhauss, 2008). Moreover, our experiments with inverted larvae reveal that when both signals are presented in opposition to one another, they are combined by the oculomotor system in such a way as to improve gaze stabilisation compared to the performance of the vestibular system alone. Therefore, the larval zebrafish may disambiguate utricular inputs by utilising sensory information from at least one other modality, vision. In addition, we speculate that visual feedback could drive plasticity within the fundamental VOR circuit of larval fish (Miles & Lisberger, 1981); the simplicity of this circuit combined with the ability to perform functional imaging in zebrafish and utilize an array of molecular-genetic tools (Orger et al., 2008; Schoonheim et al., 2010; McLean & Fetcho, 2011; Miri et al., 2011) will make this an exciting question for future studies.

By the time zebrafish are one month old, their semicircular canals become large enough to function. Our work highlights a fascinating developmental challenge: incorporation of an entirely new sense organ within an existing functional scaffold. Comparable challenges must have been met on an evolutionary timescale, when semicircular canals appeared in the vertebrate lineage. Thus, in developmental, and perhaps also evolutionary terms, the utricular VOR circuit serves as a blueprint for the control of vestibular responses; later developing canal-dependent

circuitry must converge with this initial template. One line of parallel evidence for such a primary, utricle-derived vestibular scaffold comes from measurements of the VOR in otoconia-deficient mice. There, even for canal-dominated input, the system is still impaired in the absence of otolith-derived information, consistent with a canal system that relies on an underlying otolith-derived structure (Harrod & Baker, 2003; Andreescu et al., 2005).

In summary, larval zebrafish perform a compensatory rotational VOR in response to changes in head orientation across a broad range of frequencies, using vestibular input from only the utricle. This behavior is dependent upon sensorimotor neurons in the tangential nucleus that process utricular inputs and control extra-ocular motoneurons. We propose that this simple three-neuron arc represents a fundamental circuit mediating gaze stabilization in vertebrates.

Acknowledgements

The authors thank Joel Greenwood and Ed Soucy for technical support, Phil Elks and Henry Roehl for kindly providing the lyn-mCherry construct, Sandeep Robert Datta for kindly providing the C3PA-GFP construct in advance of publication and Ruben Portugues for helpful discussions and critical reading of the manuscript. I.H.B is supported by a Sir Henry Wellcome Postdoctoral Fellowship from the Wellcome Trust. D.S. was supported by a Helen Hay Whitney Foundation Fellowship. Research was supported by NIH grants 1R01DA030304-01 and 1RC2NS069407-01 awarded to F.E., RC2NS069407, R01GM08535, and HL109525 awarded to A.S and EY002007 awarded to R.B.

Author Contributions

I.H.B, L.H.M and D.S designed and executed all experiments, analyzed data and wrote the manuscript. M.O. made the Tg(*alpha tubulin*:C3PA-GFP) and Tg(*elavl3*:lyn-mCherry) transgenic lines. D.R. and J.L. performed laser-ablation experiments. J.C.B. designed the apparatus and collected preliminary data. A.S, F.E and R.B conceived experiments, interpreted data and contributed to preparing this manuscript.

Figure Legends

Figure 1: Compensatory ocular counter-rotations following changes in head tilt.

(a) Definition of the pitch-tilt axis for head rotation (θ), centered about the ear. (b) Definition of the torsional axis for ocular rotation (ψ), centered at the eye. (c) Example raw eye position trace (black/colors), from a representative 10 dpf larva presented with 1.5 cycles of 10° steps covering the $\pm$ 60° range. (d) Final eye position observed for each step, for this example 10 dpf larva. Vertical lines are mean $\pm$ s.d. measured over the last 3 s of each step, grey line plots the fit to sine-transformed head rotation. (e) The average response for each colored step type from (c). Black represents the step stimulus. Data shown in both the position and velocity domains (left and right panels, respectively). (f) Gain (peak eye speed/peak head speed) for the individual steps that progressively rotated the fish from $+60°$ (nose-down) through horizontal to $-60°$ (nose-up) and then back again. Vertical lines are mean $\pm$ s.d. Colors as in (c, d). Horizontal grey line at gain 1 indicates a perfectly compensatory response, when peak eye speed matches the peak speed reached by the step (32°/s). See also Figure S1.

Figure 2: Ontogeny and bandwidth of the larval zebrafish VOR.

(a) Example eye position traces from a 3 dpf larva (top) and a 5 dpf larva (middle), experiencing 0.25 Hz sinusoidal pitch tilts and a 10 dpf larva (bottom), experiencing 2 Hz pitch-tilts. Note the phase lag of the ocular response to high freqeuncy stimuli and the complete absence of VOR behavior in 3 dpf larvae. (b, c) Bode plots of gain (b) and phase (c) of eye movement responses to sinusoidal pitch tilts across the range 0.0625–2 Hz. Data from 3 ($n = 6$), 4 ($n = 29$), 5 ($n = 34$) and 10 ($n = 18$) dpf larvae are shown as mean $\pm$ s.e.m. Traces are slightly offset to show error bars. Phase data are not shown for 3 dpf larvae because this parameter can not be accurately estimated when gain approaches zero. (d) Ribbons show the average (mean $\pm$ s.e.m.) response for fish of different ages to a single step change ($-20°$ to $-30°$, nose up) in terms of both position (left) and velocity (right). (e) Gain as a function of step position for fish of different ages. Vertical lines are the mean $\pm$ s.e.m across fish of a given age: 3 dpf, $n = 6$; 4 dpf, $n = 16$; 5 dpf, $n = 6$; 10 dpf, $n = 6$. # indicates the example step shown in (d). See also Figure S2.

Figure 3: Linear summation of bilateral utricular inputs.

(a) Lateral view of a 5 dpf larva (anterior left). Arrow points to the utricular otolith. (b) Surgical removal of the utricular otolith. Note the collapse of the otic vesicle following surgery. (c) Example traces from a representative fish (left eye), showing torsional eye movement responses to a 0.25 Hz sinusoidal stimulus following sequential perturbations: baseline performance before surgery, after

removal of only the left otolith, after both otoliths are removed, and after both are removed and tilt stimuli were delivered in the light (in all other cases fish were tested in the dark). (d) Bode plots of gain and phase for utricle removal experiments. Lines with open symbols represent right eye data, lines without represent left eye data. We combined data for experiments in which the left otolith was removed first ($n = 6$) and in which the right otolith was removed first ($n = 4$) because for both eyes, removal of either otolith had similar effects. Data are shown as mean $\pm$ s.e.m. Phase data are not shown for the 'Bilateral removal (dark)' condition because this parameter can not be accurately estimated when gain approaches zero. See also Figure S3 and Movie S1.

Figure 4: Changes in vertical eye position after unilateral utricle inactivation.

(a) Schematic representation of the vertical eye positions that were measured under different experimental conditions. By viewing the larvae head-on, the long axes of the right (red) and left (blue) eyes were measured to determine vertical eye position. Orthogonal visual axes are shown in gray and the predicted superior extraocular muscle forces are shown in orange, and inferior muscle forces in green. (b) Summary vertical eye position data, presented as median $\pm$ interquartile range for experiments in which the left utricular otolith was removed first (left panel, $n = 10$) or the right otolith was removed first (right panel, $n = 4$). See also Movie S2.

Figure 5: Tangential neurons project from the octavolateral hindbrain to contralateral extra-ocular motoneurons.

(a, b) Projections of two-photon image stacks showing the morphology of tangential neurons in 6 dpf larvae, which were labeled by focal electroporation. (a) An Ascending tangential neuron with a cell body in the right tangential nucleus. (b) An Ascending/Descending neuron and a Commissural neuron, both with soma in the right tangential nucleus. (c–f) Double retrograde labeling of the same larvae shown in (a, b). Fluorescent dextrans were applied to the rostral spinal cord to label reticulospinal neurons (blue), and to the orbit to label extraocular motoneurons (red). (c) The cell body of the Ascending neuron is visible in lateral rhombomere (r) 5, immediately caudal to the vestibulo-spinal (VS) neurons in r4. M indicates the Mauthner cell. Axon terminal arbors are located in nIII, nIV and the nucleus of the MLF (nMLF) on the opposite side of the brain, shown at higher magnification in (e). (d) Double retrograde labeling showing the projection patterns of the neurons in (b). The Commissural neuron projects to the contralateral vestibular field. The Ascending/Descending neuron extended axon collaterals into various parts of the reticular scaffold in additional to the rostral arborizations adjacent to the ocular motoneurons and the nMLF (shown at higher magnification in f). (g) Two-photon projections of individual tangential neurons, overlaid and color-coded to show the stereotypical morphology of Ascending (black, $n = 5$), Ascending/Descending (red, $n = 4$) and Commissural (blue, $n = 2$) subtypes. Images

were manually scaled and aligned to allow comparison of cell morphologies. All of the Ascending and Ascending/Descending neurons projected to ocular motonuclei on the contralateral side of the brain. All images are dorsal views, anterior right. Scale bars represent 10 μm for a, c and 50 μm for b, d–f. See also Figure S4, Movie S3 and Movie S4.

Figure 6: Tangential nucleus neurons are required for the VOR.

(a–c) Labeling of the tangential nucleus with C3PA-GFP in a lyn-mCherry background. (a) Lyn-mCherry expression (red) revealed the location of the Mauthner cell (M) and vestibulo-spinal neurons (VS), which served as landmarks allowing us to target the tangential nucleus (Tan) in r5. (b) After photoactivation, a cluster of cells in the left Tan nucleus is visible (white). (c) Axonal projections to nIII, nIV and nMLF were visible after bilateral labeling of tangential nuclei. The yellow arrow indicates axons ascending in the left MLF, derived from right-sided photoactivated Tan neurons. Insets show the photoactivated tangential nuclei, with dynamic range adjusted to reveal the cell bodies. (d) Three optical sections through the right tangential nucleus of the same larva shown in (c). Photolabeled neurons were individually ablated by spiral-scanning a pulsed infrared laser beam that was centered on the somata of each neuron in turn (red spots). (e) Laser-ablation of C3PA-GFP-labeled tangential neurons caused a substantial reduction in the gain of the VOR. Left panel shows Bode plot of gain, presented as median $\pm$ interquartile range ($n = 12$). Middle panel shows change in mean gain across frequencies for all 12 larvae. Right panel shows Bode plot of phase. (f) Data from two fish that displayed the greatest reduction in gain after tangential ablation. Data shown as mean $\pm$ s.e.m. Torsional eye rotations could be evoked by visual input at low frequencies. All images are dorsal views, anterior right. Scale bars represent 50 μm. See also Figure S5.

Figure 7: Interaction between visual and vestibular signals in the control of compensatory eye movements.

(a) Schematics illustrating the direction of gravitational forces acting on the utricle in upright (black) versus inverted (green) fish, in response to the same change in table pitch (nose-down for the upright fish). The earth-horizontal force component deflecting utricular hair cells acts in opposite directions under these two conditions. However, in both cases, the appropriate compensatory torsional rotation of the left eye should be a clockwise rotation. (b) Example traces from a representative larva experiencing a 0.25 Hz sinusoidal oscillation (gray). In the normal upright condition (black trace) eye rotations were compensatory, but rotations were of opposite sense when the fish was inverted (green trace). When inverted fish were tilted in the light, the gain of the torsional rotations was reduced (orange trace). (c) Bode plots showing gain and phase of eye movement responses under different conditions. Seven fish were tested in both upright

(black) and inverted (green) orientations. Four of these were additionally tested when inverted and in the light (orange). All data are from 5 dpf larvae and are shown as mean ± s.e.m. Traces are offset slightly to show error bars. See also Movie S5.

Figure 8: Oculomotor circuitry in larval zebrafish.

Schematic of the three-neuron circuit that we propose mediates the VOR in larval zebrafish and parallel circuitry that controls horizontal saccades. Utricular afferent neurons project into the CNS via the VIIIth nerve and terminate in the octavolateral neuropil of the hindbrain. Tangential neurons, located in rhombomere 5, elaborate dendritic arbors in the octavolateral neuropil and project axons to the contralateral side of the brain. Tangential neurons have axon terminal arbors within nIII and nIV cranial motor nuclei, which contain extra-ocular motoneurons that innervate superior and inferior eye muscles of the contralateral and ipsilateral eyes, respectively. Thus, this circuit mediates compensatory eye rotations in response to pitch and rolls tilts. Parallel oculomotor circuitry controls horizontal saccades: burst generator neurons, also located in rhombomere 5, activate ipsilateral abducens motoneurons and contralateral oculomotor motoneruons (via abducens internuclear neurons) resulting in contraction of the ipsilateral lateral rectus and contralateral medial rectus.

Figure S1: Apparatus for measuring the VOR and accompanying example data, (related to Figure 1).

(a) Schematic of the tilting apparatus with the rotation axis centered at the head of the fish. (b) Examples of raw data traces, showing torsional movements of the left eye in response to sinusoidal pitch-tilts at 0.125 Hz. Insets show individual images from the camera at the indicated times (red dashed lines) and schematics represent the activity of the extraocular muscles that produce either clockwise (CW) or counter-clockwise (CCW) torsional eye rotation. Abbreviations: SR, superior rectus; SO, superior oblique; IR, inferior rectus; IO, inferior oblique.

Figure S2: The gain of the VOR varies with peak angular velocity, (related to Figure 2).

(A) Bode plots of gain (left) and phase (right) for VOR responses to sinusoidal pitch-tilts which had constant amplitude (5°) but varied in frequency and peak angular velocity. Data are from 5 dpf larvae, $n = 12$. Performance improves at higher frequencies/angular velocities and approaches a plateau at 0.5 Hz (corresponding to 15.7°/s). Note that in these preliminary experiments we used larvae of a different wild-type background, which displayed higher gain than the AB background used for most other experiments. (B) Peak angular velocity at each sinusoidal

frequency (amplitude 5°). Note that for most experiments we delivered sinusoidal oscillations across this same frequency range but with *constant* peak velocity (15.7°/s) and varying amplitude.

Figure S3: Control lesions minimally influenced the gain of the VOR, (related to Figure 3).

(a) Bode plot showing that collapse of the otic vesicle (sham surgery; gray) had little effect upon torsional eye rotations, whereas removal of either one or both utricular otoliths substantially reduced gain (blue and green traces). Data collected from 5 dpf larvae and represented as mean $\pm$ s.e.m., $n = 4$.

Figure S4: Retrograde dye tracing from the orbit labels nIII and nIV, (related to Figure 5).

Confocal *z*-projection of the midbrain and hindbrain of a 6 dpf Tg(*isl1*:GFP)^{rw0} transgenic larva (GFP expression shown in green) following retrograde dye tracing from the orbit (red). Extraocular motoneurons in both the oculomotor and trochlear motor nuclei, which innervate eye muscles mediating torsional eye rotations, were labelled. In addition, in this specimen, one abducens motoneuron (ventral to nVII, arrowhead) as well as several trigeminal motoneurons were back-filled. Dorsal view, anterior right. Abbreviations: nIII, oculomotor nucleus; nIV, trochlear nucleus; nVa, nVp, anterior and posterior clusters of trigeminal motor neurons.

Figure S5: Laser ablation of single, identified, tangential nucleus neurons, (related to Figure 6).

Two examples showing targeted laser-ablation of tangential nucleus neurons. (a, e) Images of single *z*-planes following photoactivation of the tangential nucleus, with red targeting spots indicating locations near the center of selected cells where the pulsed infrared laser was spiral-scanned. (b, f) Images immediately after ablation showing disrupted fluorescence caused by cavitation bubbles within the targeted neurons (red spots). (c, d, g) Confocal images after fixation and TO-PRO-3 staining. We were able to locate the autofluorescent signature of cavitation bubbles (which appear as green crescent-shaped structures, arrowheads). These lesion sites were associated with an absence of nuclear staining, whereas immediately adjacent cells displayed intact nuclei (red). (c) and (d) are two different *z*-planes, in the same specimen, in which we located the four cavitation bubbles corresponding to four ablated tangential neurons. All images show dorsal views of the left tangential nucleus region, anterior top. Two examples are shown from a total of six larvae.

Movie S1: Spontaneous saccades after surgical removal of the utricular otoliths, (related to Figure 3).

Movie S2: Vertical eye position after unilateral otolith removal, (related to Figure 4).

Movie S3: An Ascending tangential neuron, (related to Figure 5).

Movie S4: A Commissural and an Ascending/Descending tangential neuron, (related to Figure 5).

Movie S5: VOR behavior in inverted larvae, (related to Figure 7).

Experimental Procedures

Fish

Zebrafish (*Danio rerio*) of the wild-type AB strain were used for all experiments unless otherwise stated. For labeling of tangential nucleus neurons by focal electroporation, we used the *mitfa*$^{w2/w2}$ skin pigmentation mutant (Lister et al., 1999) to allow better visualization during cell labeling and imaging.

To generate the transgenic line Tg(*alpha tubulin*:C3PA-GFP) the C3PA-GFP open reading frame and polyadenylation sequence (Ruta et al., 2010) was PCR amplified using the primers cttttgccttttttcttcacagGTGAGCAAGGGCGAGGAGC (forward, coding sequence upper case) and GGggatccTGGACAAACCACAACTAG (reverse) and fused in a second PCR step to the goldfish alpha1-tubulin cis regulatory sequence (Hieber et al., 1998), and first exon and intron amplified with the forward primer ggACGCGTgctcccggactcagatc and complementary reverse primer GCTC-CTCGCCCTTGCTCACctgtgaagaaaaaggcaaaag, resulting in an in frame replacement of the alpha tubulin coding sequence with C3PA-GFP. This cassette was cloned into a plasmid with Tol2 arms using restriction enzymes Mlu1 and BamH1. The transgenic line Tg(*elavl3*:lyn-mCherry) was made by amplifying mCherry sequence fused to the N-terminal membrane targeting domain of the lyn kinase (kindly provided by Henry Roehl), and downstream polyadenylation sequence using the primers ggcctctcgagcctctaga (forward) and aatgcattggcgccgcgg (reverse). This was first cloned downstream of a attR1-R2 cassette flanked by tol2 sites using the enzymes Xba1 and SacII, and subsequently placed downstream of elavl3 cis-regulatory elements including the first exon with mutated start codon, and first intron (Higashijima et al., 2003), via LR recombination (Invitrogen) with an attL flanked elavl3 entry clone. The resulting plasmids were injected into 1 cell-stage embryos at a concentration of 20 ng/μl in combination with tol2 mRNA at a concentration of

30 ng/μl. Founders were selected based on high, and spatially even expression.

Fish were reared on a 14/10 h light/dark cycle at 28°C. Animal handling and experimental procedures were approved by the Institutional Animal Care and Use Committee of New York University School of Medicine (New York, NY, USA), Cornell University (Ithaca, NY, USA) and the Harvard University Standing Committee on the Use of Animals in Research and Training.

Behavioral experiments

Mounting of the fish was done as per (Beck et al., 2004a). Briefly, larvae were restrained in 2% low-melting temperature agarose (Invitrogen), which was dissected away to free the head, stopping at the middle of the otic vesicle. The agarose block was pinned to a small piece of Sylgard 182 (Dow Corning, Midland MI), which was then pinned in a larger custom glass chamber (25 mm square) filled with 30% Danieau's solution (17.4 mM NaCl, 0.21 mM KCl, 0.12 mM $MgSO_4 \cdot 7\,H_2O$, 0.18 mM $Ca(NO_3)_2$ and 1.5 mM HEPES, pH 7.2), and covered with a coverslip held in place with vacuum grease. The chamber was securely mounted in a custom holder on a micro-manipulator, attached to the base of the tilting platform and position was adjusted such that the head of the larvae was aligned with the rotation axis of the apparatus. For delivering pitch-tilts, the anterior-posterior axis of the larvae was perpendicular to the rotation axis of the apparatus. For delivering roll-tilts, the anterior-posterior axis of the larvae was aligned to the rotation axis of the apparatus.

The custom-built tilting apparatus consisted of a rotating platform driven by a DC motor. Software, custom-written in LabVIEW 2010 (National Instruments, Austin, TX) was used to send command signals to the DC motor and record platform velocity via a tachometer coupled to the rotation axis. A high-speed camera (Pike F-032, Allied Vision Technologies), mounted on the rotating platform and centered upon the axis of rotation, was used to image the eye of the larva at 50–100 Hz under infra-red illumination, which was provided by six 850 nm LEDs (IR-1W-850, superbrightleds.com). Torsional eye position was extracted from the video stream by comparing each individual image of the eye, viewed from the side, to a reference image that was recorded at 0° (platform horizontal), using the LabVIEW "IMAQ Match Pattern" algorithm. Counter-clockwise rotations of the left eye were classed as positive angles. Vertical eye position was measured by fitting an ellipse to the image of the eye and determining the angle between the long-axis of the ellipse and the dorso-ventral axis of the larva. Both both eyes, positive angles were measured for rotations of the upper pole of the eye towards the left ear.

Analysis of behavioral data

All data analysis was done using custom software written in MATLAB (Mathworks, Natick, MA). Each eye movement trace was analyzed manually to select sections where spontaneous horizontal

saccades or jaw movements had not disrupted the recorded eye position. For pitch-tilt steps, individual steps were rejected if the entire 5 s eye movement trace was unstable. Occasionally, the computational demands of pattern matching were such that the rate fell below 50 Hz; the pitch steps were fit with a cubic spline and interpolated to allow comparison across fish. For sinusoidal data, eye position and platform position were fit with sinusoids and the amplitude and phase of the sinusoidal fits was compared to determine gain and phase shift. We used an F-test to compare each sinusoidal fit of eye position to a straight line with a slope of zero; if the sinusoid failed to produce a significantly better fit (at 99% confidence) we recorded a gain of zero and the phase shift was undefined. The final estimate of the gain and phase for a recording was the median of the gain and phase values for the different sections from that recording. To evaluate changes in vertical eye position, we analyzed recordings where larvae were sinusoidally roll-tilted at 0.25 Hz and extracted mean vertical eye position as a measure of the vertical null position of the eye. For statistical analyses we performed ANOVA, with post-hoc pairwise tests corrected for multiple comparisons (Tukey-Kramer method). All data sets adequately approximated a Normal distribution (Kolmogorov-Smirnov test). Statistical significance was considered at a 95% confidence limit.

Utricular otolith removal

Larvae were anesthetized using 0.003% MS-222 (Sigma) and a sharp tungsten pin was used to puncture the lateral wall of the otic vesicle and detach the utricular otolith from the underlying sensory maccula. In control surgeries, the otic vesicle was punctured but the otolith was not removed. After surgery, larvae were returned to 30% Danieau's solution to recover, and behavior was measured after 1.5 h.

Focal electroporation

Focal electroporation was performed as detailed in (Tawk et al., 2009). Briefly, larvae were anesthetized and mounted in low-melting temperature agarose in a custom chamber. Micropipettes having a tip diameter of 1–2 μm were filled with a solution containing plasmid DNA dissolved in distilled water at a concentration of 1 $\mu g/\mu l$. The plasmid was based on the pCS2 expression construct and encoded GFP with an N-terminal GAP43 membrane localization sequence. Micropipettes were positioned at the extreme lateral limit of rhombomere 5, at the same dorsoventral level as the Mauthner axon midline crossing, which is visible under transmitted light illumination on a compound microscope. Three 250 ms trains of voltage pulses were delivered, with 1 s interval between trains, using a Grass SD9 stimulator (Grass Technologies). For each train, pulses had an amplitude of 30 V, a 2 ms on time and were delivered at 200 Hz. Following electroporation, larvae were allowed to recover overnight. The next day, larvae containing labeled

neurons were anesthetized and mounted in agarose and imaged using a custom-built 2-photon microscope with 920 nm excitation and a standard GFP bandpass filter (FF01-510/84, Semrock).

Photoactivation of C3PA-GFP

Larvae (4 dpf) were generated by crossing Tg(*alpha tubulin*:C3PA-GFP) $\times$ Tg(*elavl3*:lyn-mCherry) and were selected for expression of both transgenes on a standard epifluorescence dissection microscope. Even prior to photoactivation, larvae expressing C3PA-GFP have a dim green appearance allowing them to be identified. Larvae were anesthetized using 0.003% MS-222 (Sigma) and mounted in 2% low-melting temperature agarose. A custom-built 2-photon microscope was used to photoactivate C3PA-GFP in a small volume of rhombomere 5. The photoactivation region was selected by imaging mCherry fluorescence with 800 nm excitation light and a standard emission filter set (FF01-641/75, Semrock). This allowed visualization of anatomical landmarks in the larval hindbrain, including the Mauthner cell and vestibulo-spinal neurons in rhombomere 4, enabling targeting of the tangential nucleus in ventrolateral rhombomere 5. We scanned continuously over a 25 (x) $\times$ 25 (y) $\times$ 30 (z) μm volume at 790 nm, 6 mW at sample, for 4–7 min, to photoactivate C3PA-GFP. Before and after photoactivation, we imaged GFP fluorescence in the hindbrain with 920 nm excitation and a standard GFP bandpass filter.

Laser ablation of tangential nucleus neurons

Larvae (5 dpf), in which the tangential nucleus had been labeled by photoactivation of C3PA-GFP, were first tested for baseline VOR performance. The ablation procedure was similar to that described by (Orger et al., 2008). Briefly, larvae were anesthetized and individual tangential nucleus neurons were targeted one at a time, using a pulsed infrared laser at 900 nm. A spiral-scan waveform was delivered, centered at the middle of the selected neuron, and laser power was increased until a high-amplitude signal (likely representing plasma formation) was detected on the photomultiplier tube, at which point the laser was shuttered in < 10 ms. After ablation, larvae were allowed to recover and VOR performance was tested after 3 h. To assess the efficacy of the ablation procedure, some larvae were fixed immediately after laser ablation, by incubation in 4% PFA in PBS at 4°C for 8 h. Larvae were then permeabilised by 2 x 30 min washes in PBT (0.8% Triton X-100 in PBS), followed by 35 min incubation in Proteinase K (1:1000). Larvae were incubated in TO-PRO-3 nucleic acid staining solution (Invitrogen; 1 μM in PBT) for 2 h, washed in PBT and imaged on a Zeiss LSM 710 laser-scanning confocal microscope with 488 nm and 633 nm lasers and a 20$\times$ objective lens.

Dye labeling of reticulospinal and oculomotor neurons

Larvae were anesthetized and mounted in low-melting temperature agarose as described above. Tungsten needles were used to place crystals of 10 kD dextran, conjugated to AlexaFluor-594 or 647 (Invitrogen) within a lesion site within the spinal cord at the level of myotome 5 or in the orbit. Fish were subsequently transferred to modified artificial cerebrospinal fluid (ACSF; 67 mM NaCl, 2.9 mM KCl, 10 mM HEPES, 2.1 mM $CaCl_2$, 1.2 mM $MgCl_2$, 10 mM glucose, 164 mM sucrose, pH 7.5, 323.8 mOsm) for 3 h to allow time for retrograde movement of the dye within axons (Ma et al., 2009). For imaging, the brain was exposed by dissecting off the overlying skin with a sharp tungsten needle and confocal image stacks were acquired using a Zeiss LSM 710 laser-scanning microscope.

Image analysis

Confocal and 2-photon image stacks were processed using ImageJ (NIH) and Photoshop CS5 (Adobe).

References

Andreescu, C. E., De Ruiter, M. M., De Zeeuw, C. I., & De Jeu, M. T. G. (2005). Otolith deprivation induces optokinetic compensation. J Neurophysiol, 94, 3487–96.

Angelaki, D. E. (2004). Eyes on target: what neurons must do for the vestibuloocular reflex during linear motion. J Neurophysiol, 92, 20–35.

Angelaki, D. E. & Cullen, K. E. (2008). Vestibular system: the many facets of a multimodal sense. Annu Rev Neurosci, 31, 125–50.

Angelaki, D. E. & Hess, B. J. (1996). Organizational principles of otolith- and semicircular canal-ocular reflexes in rhesus monkeys. Ann N Y Acad Sci, 781, 332–47.

Angelaki, D. E., McHenry, M. Q., Dickman, J. D., Newlands, S. D., & Hess, B. J. (1999). Computation of inertial motion: neural strategies to resolve ambiguous otolith information. J Neurosci, 19, 316–27.

Angelaki, D. E., Shaikh, A. G., Green, A. M., & Dickman, J. D. (2004). Neurons compute internal models of the physical laws of motion. Nature, 430, 560–4.

Beck, J. C., Gilland, E., Baker, R., & Tank, D. W. (2004a). Instrumentation for measuring oculomotor performance and plasticity in larval organisms. Methods Cell Biol, 76, 385–413.

Beck, J. C., Gilland, E., Tank, D. W., & Baker, R. (2004b). Quantifying the ontogeny of optokinetic and vestibuloocular behaviors in zebrafish, medaka, and goldfish. J Neurophysiol, 92, 3546–61.

Budick, S. A. & O'Malley, D. M. (2000). Locomotor repertoire of the larval zebrafish: swimming, turning and prey capture. J Exp Biol, 203, 2565–79.

Burgess, H. A. & Granato, M. (2007). Modulation of locomotor activity in larval zebrafish during light adaptation. J Exp Biol, 210, 2526–39.

Büttner-Ennever, J. A. & Büttner, U. (1992). Neuroanatomy of the ocular motor pathways. Baillieres Clin Neurol, 1, 263–87.

Cajal, S. R. (1908). Sur un noyau special du nerf vestibulaire des poissons et des oiseaux. Trabajos del Laboratorio de Investigaciones Biológicas de la Universidad de Madrid, 6, 1–20.

Fernández, C. & Goldberg, J. M. (1976). Physiology of peripheral neurons innervating otolith organs of the squirrel monkey. i. response to static tilts and to long-duration centrifugal force. J Neurophysiol, 39, 970–84.

Goldberg, J. M. & Fernández, C. (2011). The vestibular system. Compr Physiol 2011, Supplement 3: Handbook of Physiology, The Nervous System, Sensory Processes., pp. 977–1022.

Gottesman-Davis, A. & Peusner, K. D. (2010). Identification of vestibuloocular projection neurons in the developing chicken medial vestibular nucleus. J Neurosci Res, 88, 290–303.

Graf, W. & McGurk, J. F. (1985). Peripheral and central oculomotor organization in the goldfish, carassius auratus. J Comp Neurol, 239, 391–401.

Haddon, C. & Lewis, J. (1996). Early ear development in the embryo of the zebrafish, danio rerio. J Comp Neurol, 365, 113–28.

Harrod, C. G. & Baker, J. F. (2003). The vestibulo ocular reflex (vor) in otoconia deficient head tilt (het) mutant mice versus wild type c57bl/6 mice. Brain Res, 972, 75–83.

Hess, B. J. & Angelaki, D. E. (1999). Oculomotor control of primary eye position discriminates between translation and tilt. J Neurophysiol, 81, 394–8.

Hess, B. J. M. & Dieringer, N. (1990). Spatial organization of the maculo-ocular reflex of the rat: Responses during off-vertical axis rotation. Eur J Neurosci, 2, 909–919.

Hieber, V., Dai, X., Foreman, M., & Goldman, D. (1998). Induction of alpha1-tubulin gene expression during development and regeneration of the fish central nervous system. J Neurobiol, 37, 429–40.

Higashijima, S., Hotta, Y., & Okamoto, H. (2000). Visualization of cranial motor neurons in live transgenic zebrafish expressing green fluorescent protein under the control of the islet-1 promoter/enhancer. J Neurosci, 20, 206–18.

Higashijima, S.-i., Masino, M. A., Mandel, G., & Fetcho, J. R. (2003). Imaging neuronal activity during zebrafish behavior with a genetically encoded calcium indicator. J Neurophysiol, 90, 3986–97.

Highstein, S. M. & Holstein, G. R. (2006). The anatomy of the vestibular nuclei. Prog Brain Res, 151, 157–203.

Highstein, S. M., Kitch, R., Carey, J., & Baker, R. (1992). Anatomical organization of the brainstem octavolateralis area of the oyster toadfish, opsanus tau. J Comp Neurol, 319, 501–18.

Huang, Y.-Y. & Neuhauss, S. C. F. (2008). The optokinetic response in zebrafish and its applications. Front Biosci, 13, 1899–916.

Kimmel, C. B., Ballard, W. W., Kimmel, S. R., Ullmann, B., & Schilling, T. F. (1995). Stages of embryonic development of the zebrafish. Dev Dyn, 203, 253–310.

Lambert, F. M., Beck, J. C., Baker, R., & Straka, H. (2008). Semicircular canal size determines the developmental onset of angular vestibuloocular reflexes in larval xenopus. J Neurosci, 28, 8086–95.

Lister, J. A., Robertson, C. P., Lepage, T., Johnson, S. L., & Raible, D. W. (1999). nacre encodes a zebrafish microphthalmia-related protein that regulates neural-crest-derived pigment cell fate. Development, 126, 3757–67.

Ma, L.-H., Gilland, E., Bass, A. H., & Baker, R. (2010). Ancestry of motor innervation to pectoral fin and forelimb. Nat Commun, 1, 49.

Maruta, J., Simpson, J. I., Raphan, T., & Cohen, B. (2001). Orienting otolith-ocular reflexes in the rabbit during static and dynamic tilts and off-vertical axis rotation. Vision Res, 41, 3255–70.

McArthur, K. L. & Dickman, J. D. (2008). Canal and otolith contributions to compensatory tilt responses in pigeons. J Neurophysiol, 100, 1488–97.

McLean, D. L. & Fetcho, J. R. (2011). Movement, technology and discovery in the zebrafish. Curr Opin Neurobiol, 21, 110–5.

Miles, F. A. & Lisberger, S. G. (1981). Plasticity in the vestibulo-ocular reflex: a new hypothesis. Annu Rev Neurosci, 4, 273–99.

Miri, A., Daie, K., Arrenberg, A. B., Baier, H., Aksay, E., & Tank, D. W. (2011). Spatial gradients and multidimensional dynamics in a neural integrator circuit. Nat Neurosci.

Mo, W., Chen, F., Nechiporuk, A., & Nicolson, T. (2010). Quantification of vestibular-induced eye movements in zebrafish larvae. BMC Neurosci, 11, 110.

Moorman, S. J., Burress, C., Cordova, R., & Slater, J. (1999). Stimulus dependence of the development of the zebrafish (danio rerio) vestibular system. J Neurobiol, 38, 247–58.

Orger, M. B., Kampff, A. R., Severi, K. E., Bollmann, J. H., & Engert, F. (2008). Control of visually guided behavior by distinct populations of spinal projection neurons. Nat Neurosci, 11, 327–33.

Pastor, A. M., de la Cruz, R. R., & Baker, R. (1992). Characterization and adaptive modification of the goldfish vestibuloocular reflex by sinusoidal and velocity step vestibular stimulation. J Neurophysiol, 68, 2003–15.

Peusner, K. D. & Morest, D. K. (1977). The neuronal architecture and topography of the nucleus vestibularis tangentialis in the late chick embryo. Neuroscience, 2, 189–207.

Pompeiano, O. & Allum, J. (1988). Vestibulospinal control of posture and locomotion. Prog Brain Res, 76, 1–442.

Riley, B. B. & Moorman, S. J. (2000). Development of utricular otoliths, but not saccular otoliths, is necessary for vestibular function and survival in zebrafish. J Neurobiol, 43, 329–37.

Ruta, V., Datta, S. R., Vasconcelos, M. L., Freeland, J., Looger, L. L., & Axel, R. (2010). A dimorphic pheromone circuit in drosophila from sensory input to descending output. Nature, 468, 686–90.

Schoonheim, P. J., Arrenberg, A. B., Del Bene, F., & Baier, H. (2010). Optogenetic localization and genetic perturbation of saccade-generating neurons in zebrafish. J Neurosci, 30, 7111–20.

Straka, H. & Baker, R. (2011). Encyclopedia of Fish Physiology: From Genome to Environment, vol. 1, chap. Vestibular System Anatomy and Physiology., pp. 244–251. (San Diego: Academic Press).

Straka, H., Baker, R., & Gilland, E. (2001). Rhombomeric organization of vestibular pathways in larval frogs. J Comp Neurol, 437, 42–55.

Straka, H., Holler, S., Goto, F., Kolb, F. P., & Gilland, E. (2003). Differential spatial organization of otolith signals in frog vestibular nuclei. J Neurophysiol, 90, 3501–12.

Suwa, H., Gilland, E., & Baker, R. (1999). Otolith ocular reflex function of the tangential nucleus in teleost fish. Ann N Y Acad Sci, 871, 1–14.

Szentagothai, J. (1950). The elementary vestibulo-ocular reflex arc. J Neurophysiol, 13, 395–407.

Tawk, M., Bianco, I. H., & Clarke, J. D. W. (2009). Focal electroporation in zebrafish embryos and larvae. Methods Mol Biol, 546, 145–51.

Tomchik, S. M. & Lu, Z. (2005). Octavolateral projections and organization in the medulla of a teleost fish, the sleeper goby (dormitator latifrons). J Comp Neurol, 481, 96–117.

Uchino, Y., Sato, H., Zakir, M., Kushiro, K., Imagawa, M., Ogawa, Y., Ono, S., Meng, H., Zhang, X., Katsuta, M., Isu, N., & Wilson, V. J. (2001). Commissural effects in the otolith system. Exp Brain Res, 136, 421–30.

Figure 1 – Compensatory ocular counterrotations following changes in head tilt

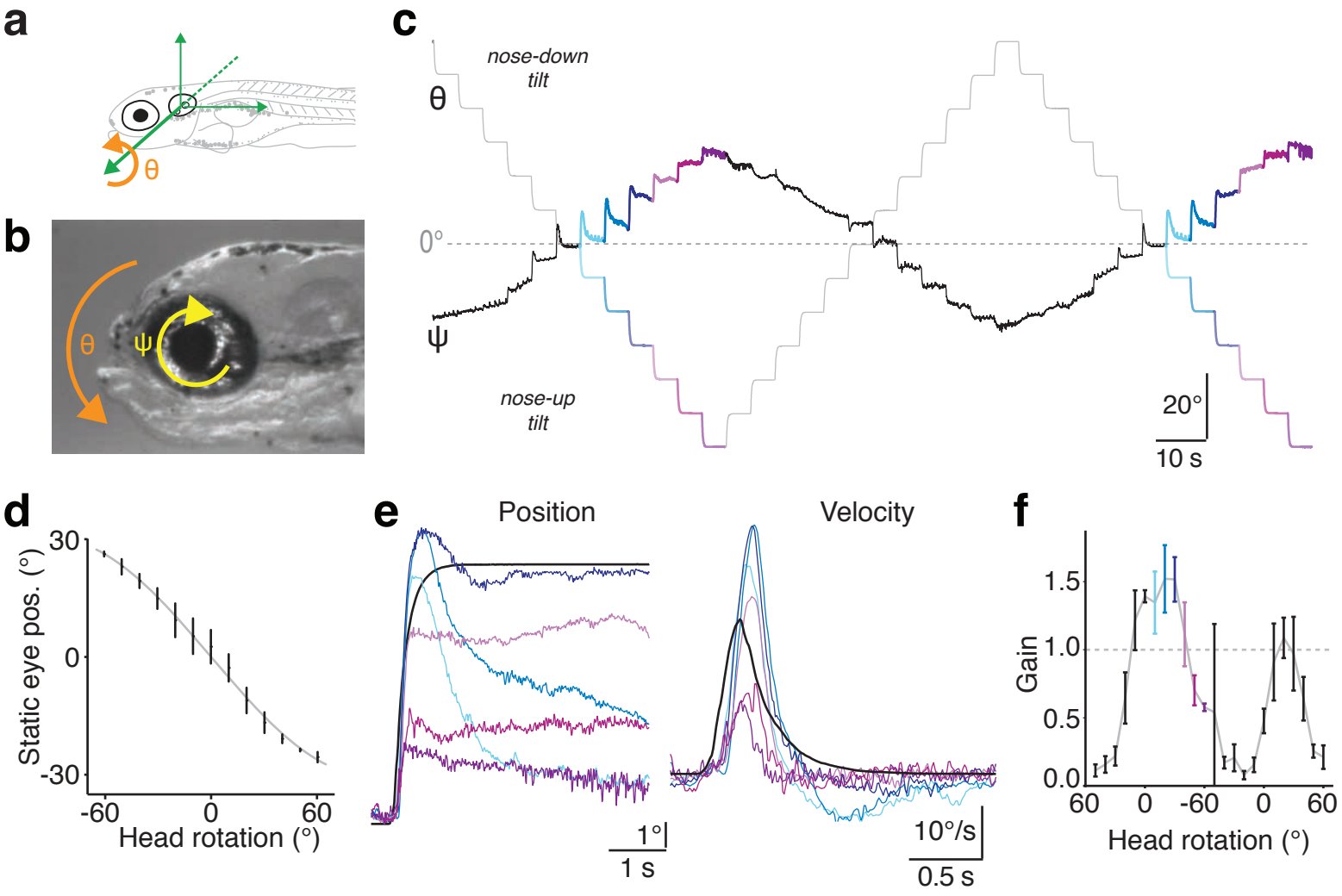

Figure 2 – Ontogeny and bandwidth of the larval zebrafish VOR

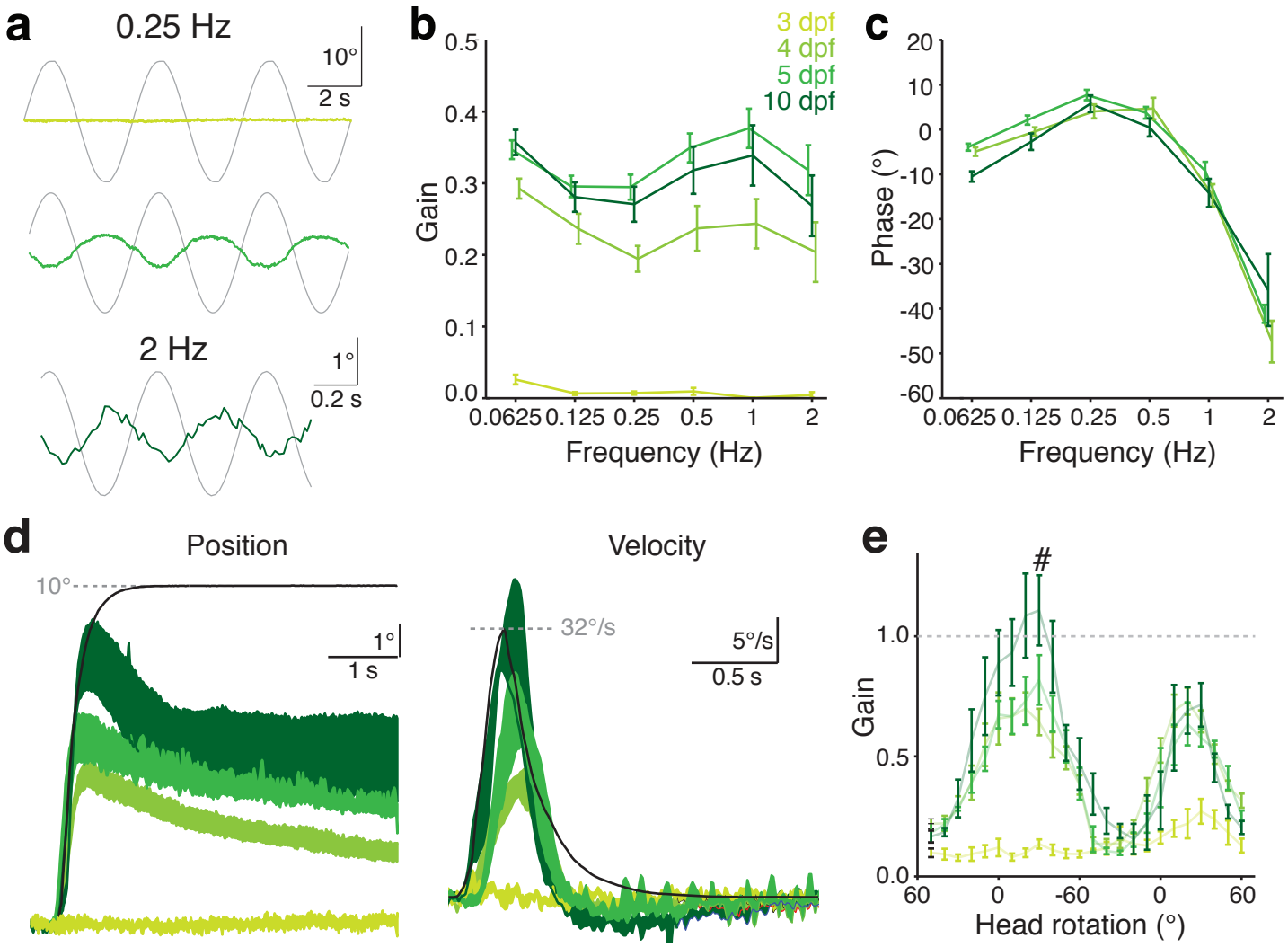

Figure 3 – Linear summation of bilateral utricular inputs

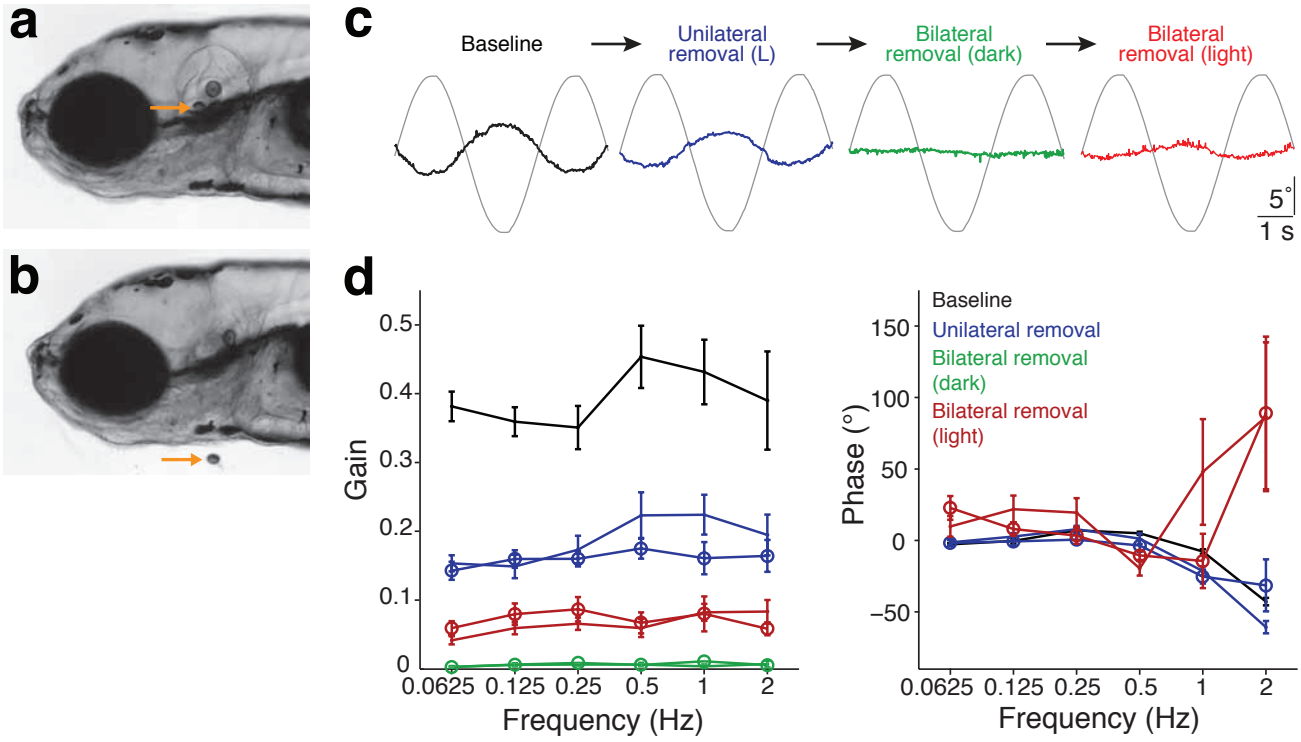

Figure 4 – Changes in vertical eye position after utricle inactivation

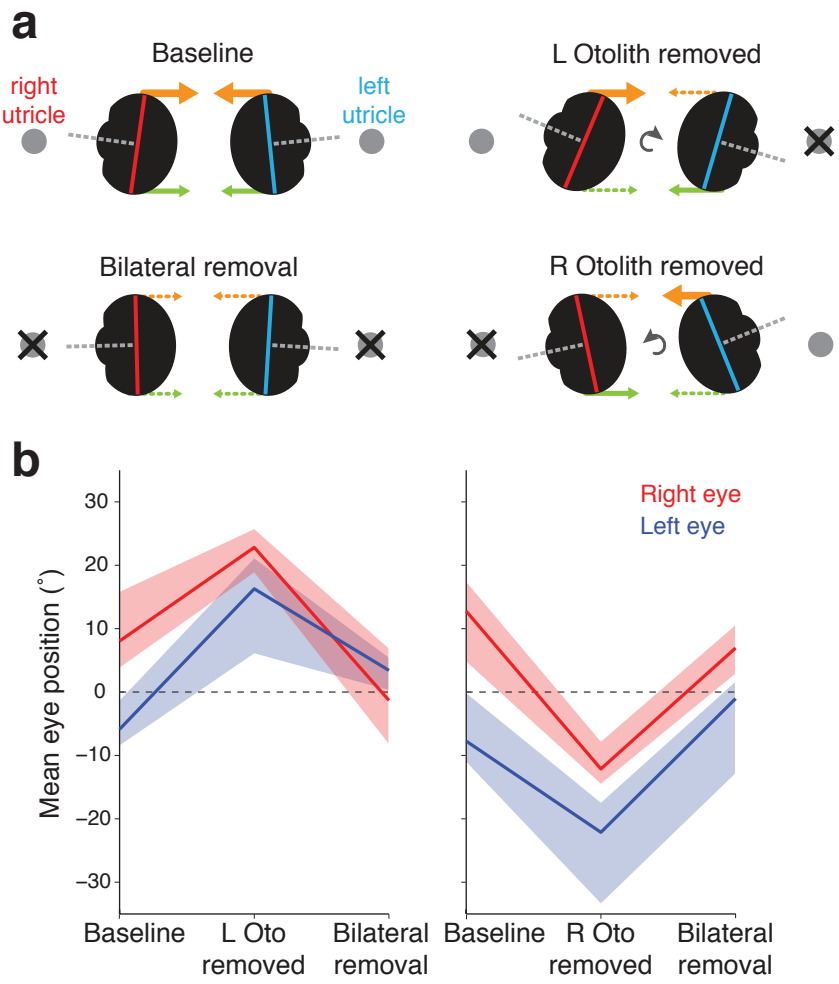

Figure 5 – Morphology of tangential neurons

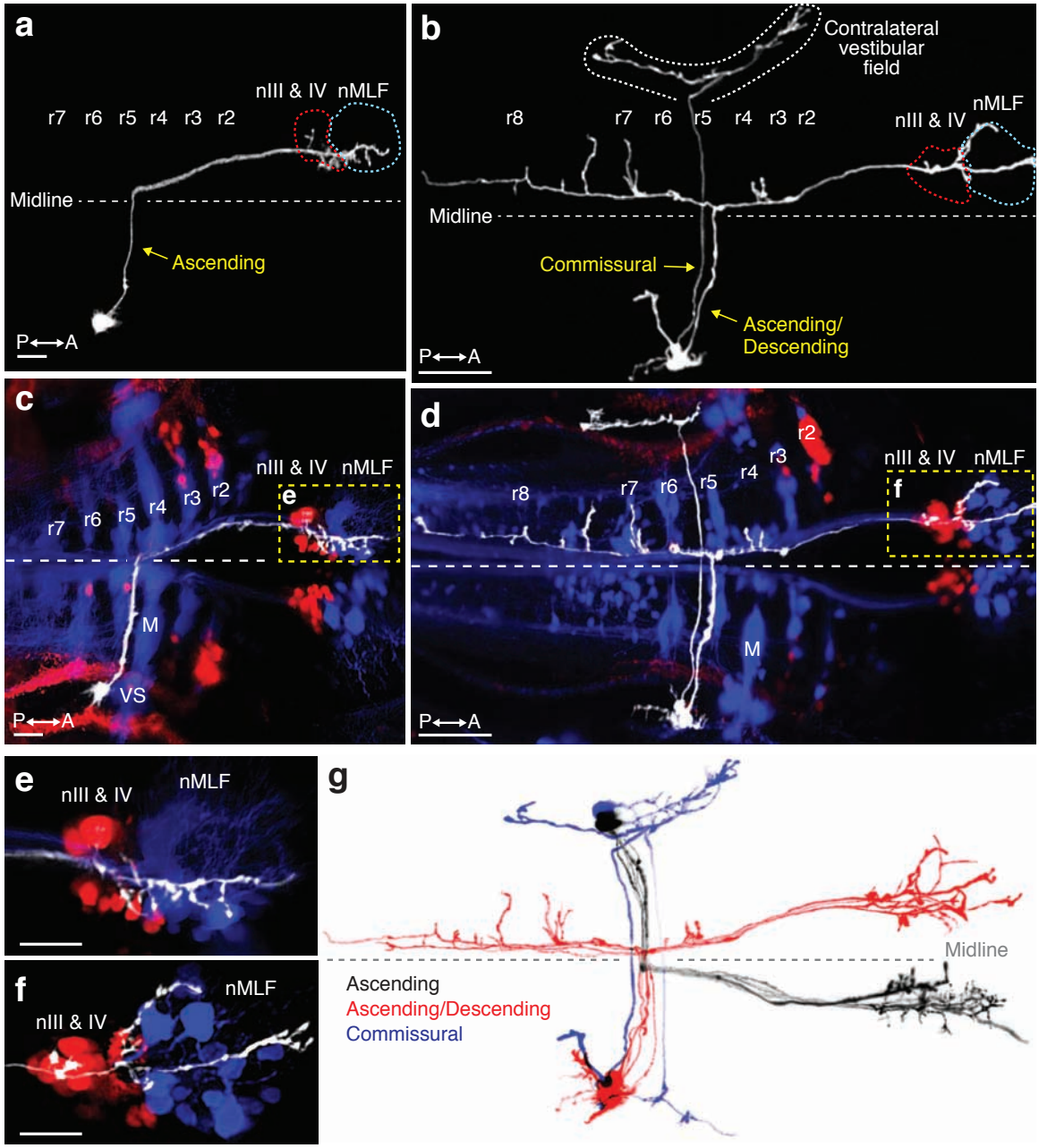

Figure 6 – Tangential neurons are required for the VOR

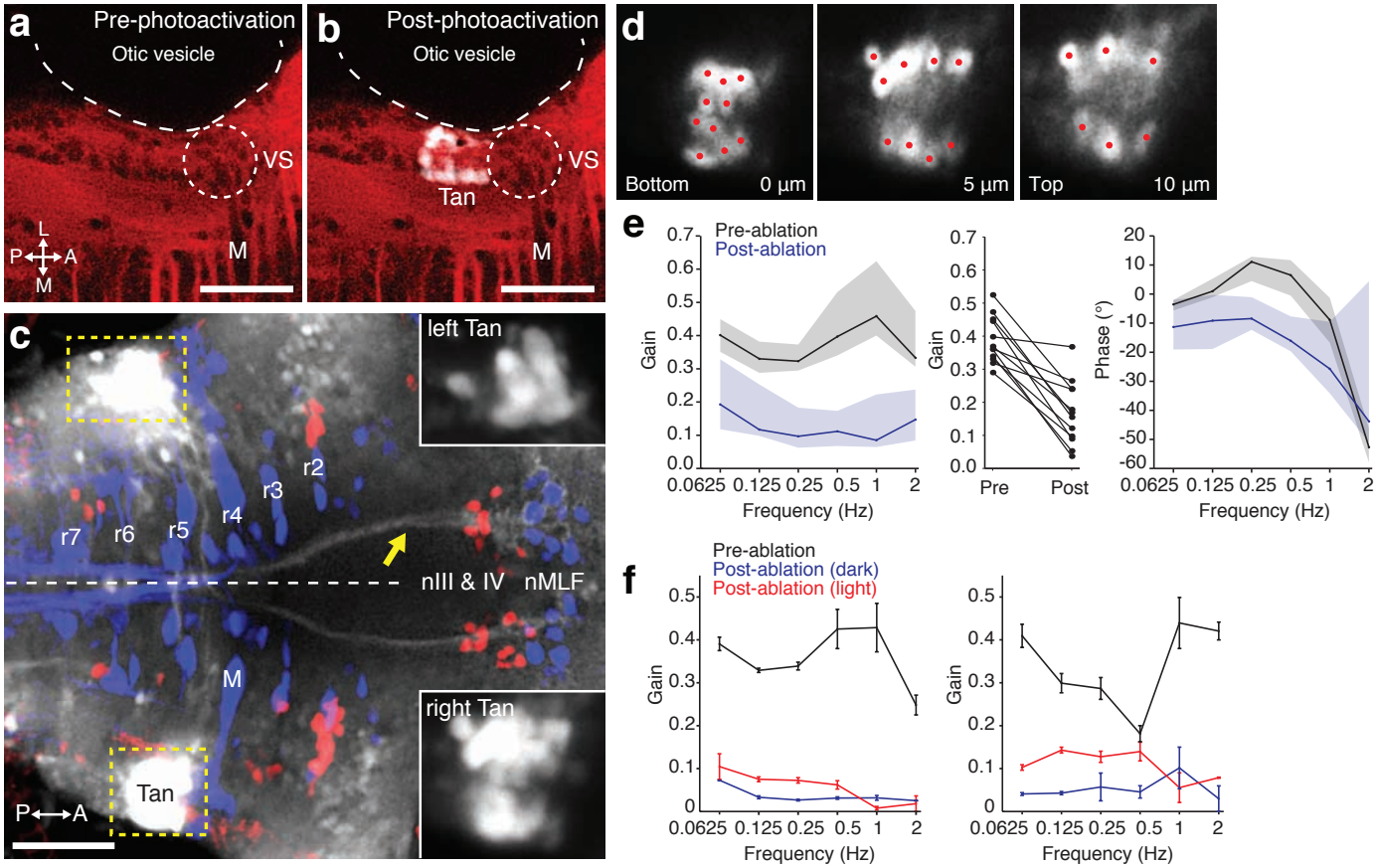

Figure 7 – Interactions between visual and vestibular inputs in the control of compensatory eye rotations

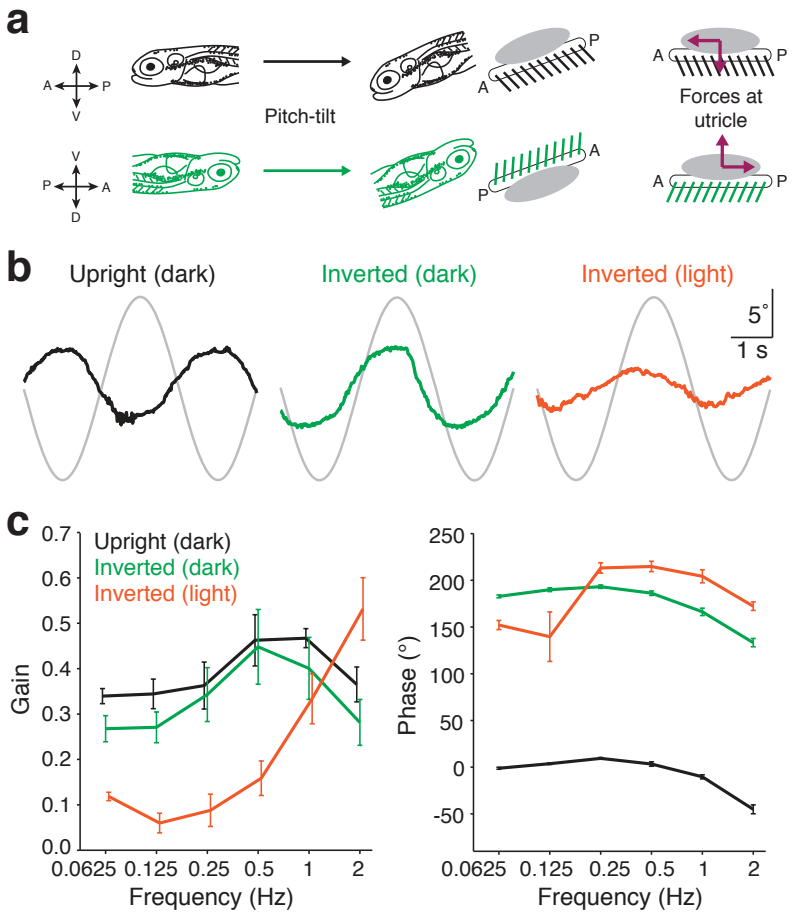

Figure 8 – Oculomotor circuitry of the larval zebrafish

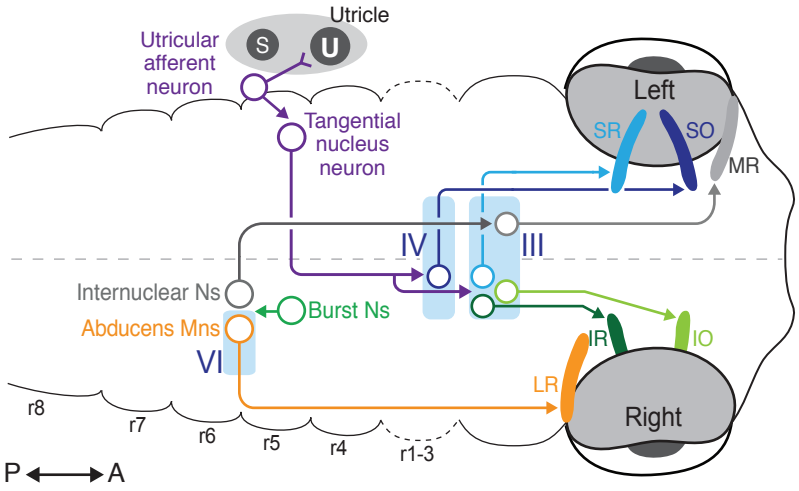

Figure S1 – Apparatus and example data

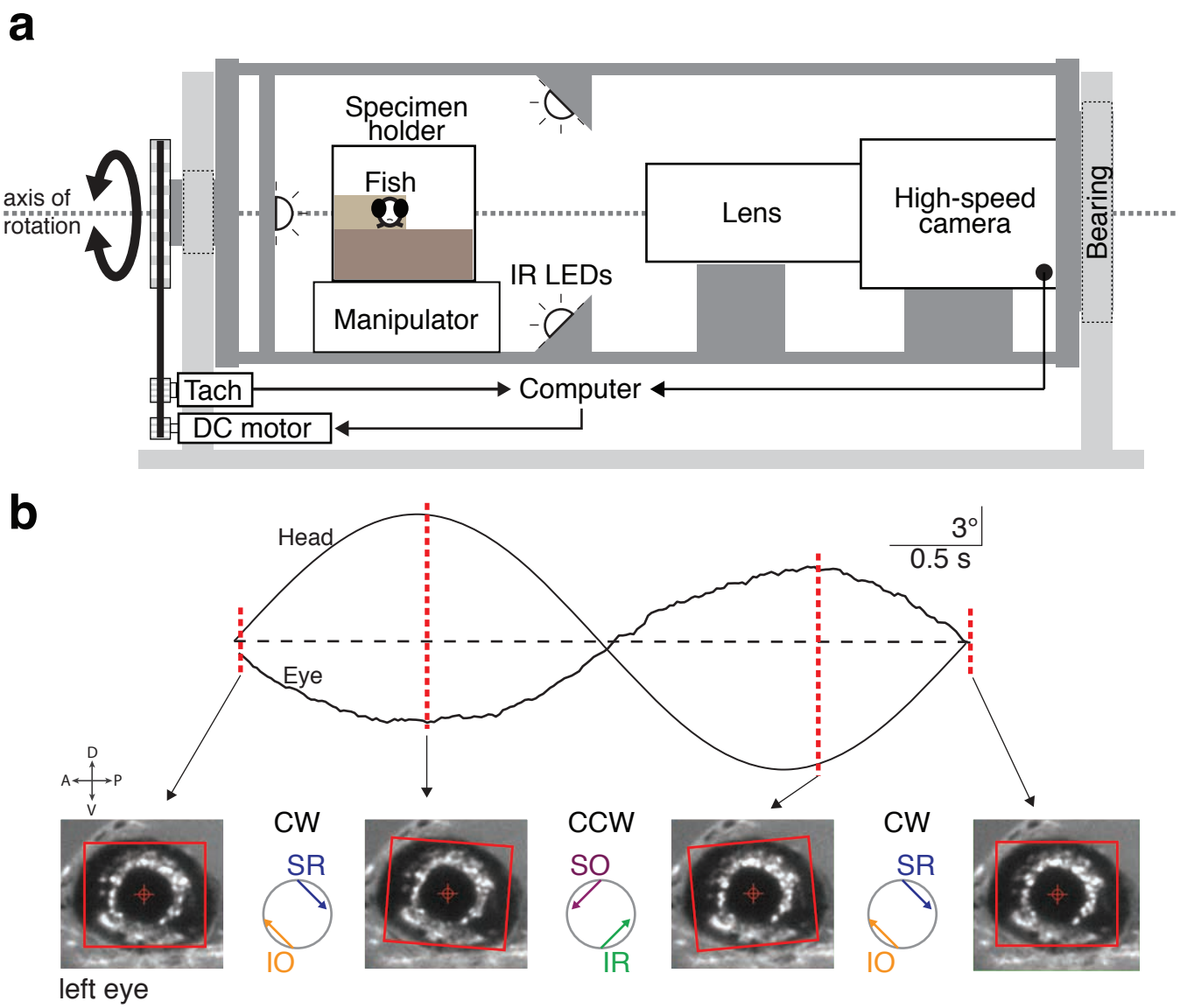

Figure S3 – VOR gain varies with peak angular velocity

a

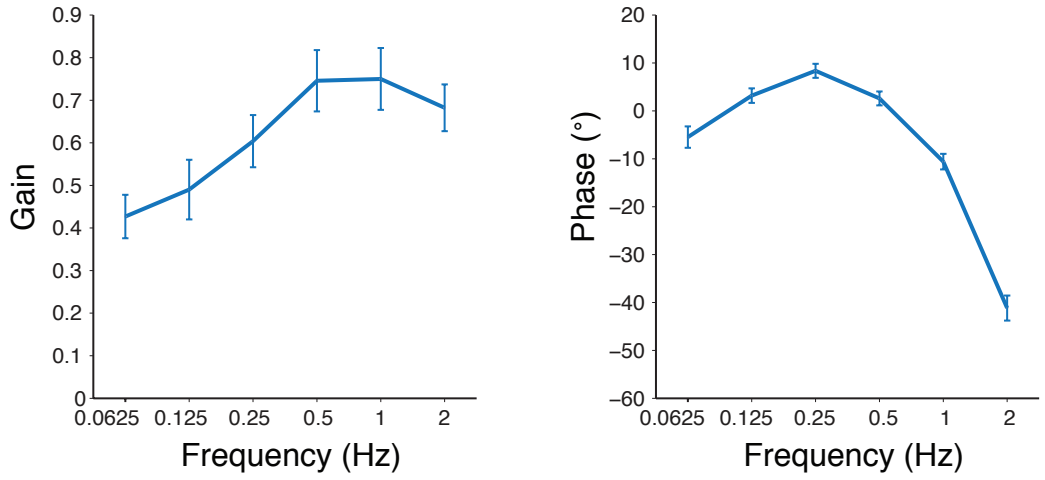

b

Frequency (Hz)	Peak velocity (˚/s)
0.0625	1.96
0.125	3.93
0.25	7.85
0.5	15.71
1	31.42
2	62.83

Figure S2 – Control surgery minimally affects the VOR

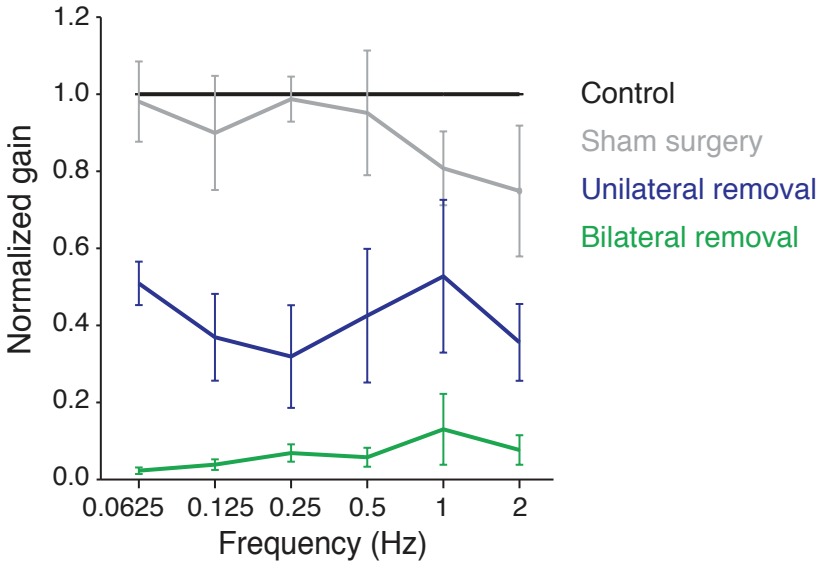

Figure S3 – Retrograde dye tracing from the orbit labels nIII and nIV

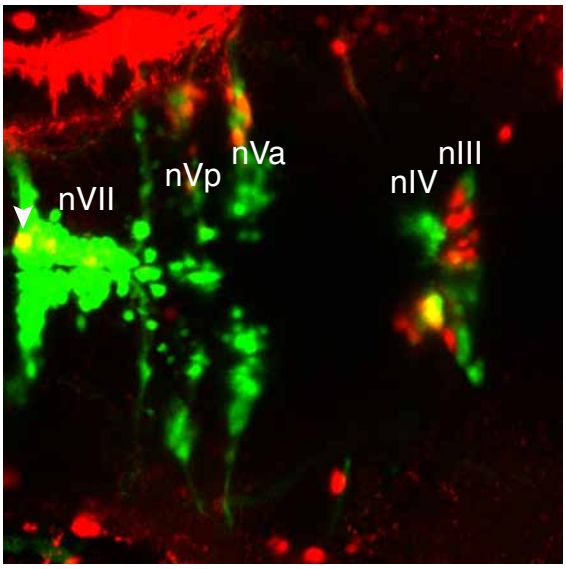

Figure S5 – Laser ablation of single tangential neurons

Fish 1

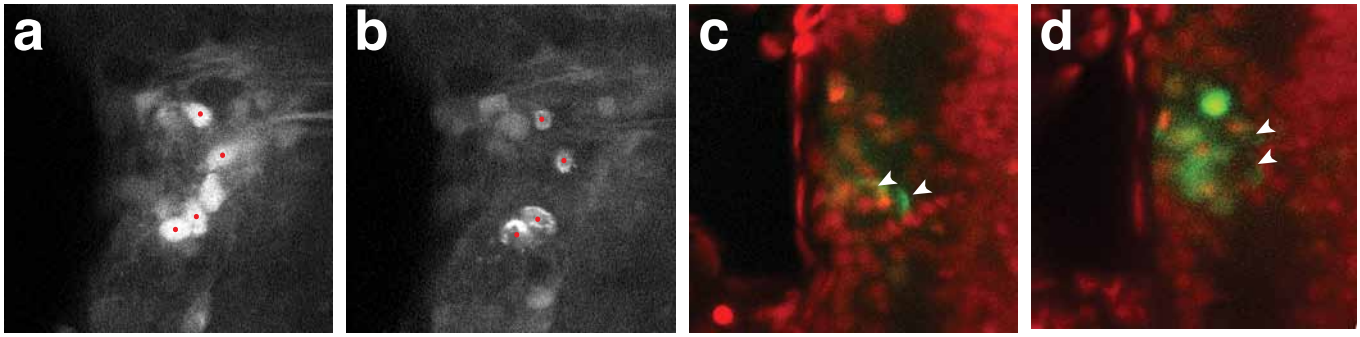

Fish 2